International Journal of Engineering and Geosciences
https://dergipark.org.tr/en/pub/ijeg
e-ISSN 2548-0960



Investigation of Longoz Forests with Remote Sensing Techniques on Google Earth Engine Platform: The Case of İğneada Longoz Forests (2000–2021)

Basak Kafes Demirci [*1], **Osman Salih Yılmaz** [2], **Fusun Balik Sanli** [3]

[1] *Yildiz Technical University, Geomatic Engineering Department, Türkiye, bsk.kfs@gmail.com*
[2] *Manisa Celal Bayar University, Demirci Vocational School, Türkiye, osmansalih.yilmaz@cbu.edu.tr*
[3] *Yildiz Technical University, Geomatic Engineering Department, Türkiye, fbalik@yildiz.edu.tr*

Cite this study: Demirci, B. K., Yılmaz O. S. , Sanl,i F. B., (2026). Investigation of Longoz Forests with Remote Sensing Techniques on Google Earth Engine Platform: The Case of İğneada Longoz Forests (2000–2021). International Journal of Engineering and Geosciences, 11(1), 78-88.

https://doi.org/10.26833/ijeg.1650786

Keywords
İğneada Longoz
Google Earth Engine
NDVI
Remote Sensing
random forest

Research Article

Received:04.04.2025
Revised:12.07.2025
Accepted:14.07.2025
Online Published:11.08.2025
Published:01.02.2026



Abstract

The study investigates changes in the İğneada Longoz forests in Kırklareli Province, Türkiye, between 2000 and 2021 using Landsat-7 and Landsat-8 satellite imagery. Classification was performed with the random forest (RF) machine learning algorithm and remote sensing (RS) techniques on the Google Earth Engine (GEE) platform. To better distinguish longoz forests and other forested areas from surrounding features, the normalized difference vegetation index (NDVI) and enhanced vegetation index (EVI) were integrated into the classification alongside standard spectral bands. In the first stage of the classification process, the study area was categorized into seven classes, identifying all forest areas. In the second stage, the area was further divided into nine classes, isolating longoz forests from other forest types. Additionally, NDVI and EVI time series analyses were conducted to evaluate forest phenology. According to the classification results, the initial stage achieved overall accuracy ranging from 79.97% to 90.63%, with an average of approximately 85.00%. The Kappa statistics varied between 0.721 and 0.877. In the second stage, the overall accuracy ranged from 75.92% to 90.04%, while the Kappa statistic was between 0.649 and 0.866.

1. Introduction

Longoz forests are ecosystems where the ground is typically submerged in water, particularly during the spring and winter seasons when rainfall is abundant. These ecosystems play a crucial role in providing breeding grounds and habitats for waterfowl, marine species, and pelagic organisms, while also supporting coastal ecological balance and biodiversity [1]. Additionally, longoz forests contribute significantly to human life by facilitating nutrient cycling, soil formation, and wood production [2]. Longoz ecosystems are highly productive and possess the unique ability to store more carbon than many other ecosystems [3]. The biomass of longoz forests in oceanic and coastal habitats is often referred to as blue carbon [4]. Globally and in Türkiye, longoz forests are recognized as ecologically significant and protected ecosystems. The İğneada Longoz forest, located within Kırklareli Province in Türkiye, hosts rich biodiversity and supports numerous endemic species.

Formed by alluvial deposits from streams originating in the Yıldız Mountains, it was designated as a National Park in 2007, becoming Türkiye 's 39th National Park. Furthermore, it is protected as a First and Second Degree Natural Protected Area.

Longoz forests possess a dynamic structure, continuously evolving under the influence of changing natural environmental conditions [5]. Their monitoring, which is essential due to their crucial role in ecological sustainability, can be effectively achieved using remote sensing (RS) techniques [6-9]. Furthermore, the normalized difference vegetation index (NDVI) has been widely applied to monitor phenological changes in forest vegetation [10]. NDVI time series, derived from the Moderate Resolution Imaging Spectroradiometer (MODIS), Landsat, and Sentinel, are extensively

employed for the periodic monitoring of long-term vegetation [11-15]. Enhanced vegetation index (EVI) also offers improved accuracy in high biomass regions by minimizing atmospheric and soil background effects [16]. In addition, the modified normalized difference water index (MNDWI) is widely used in the detection of water surfaces, especially in built-up areas, by reducing the shadow effect on water [17].

High-speed computers with large storage capacities are essential in RS studies for downloading, processing, and analysing extensive satellite image datasets [18-22]. In this context, in this respect, Google Earth Engine (GEE) is widely preferred today to overcome these difficulties [23]. GEE is a non-profit platform designed for the scientific analysis and visualization of geographic datasets, primarily for academic purposes [24–29]. In addition to providing simultaneous access to various free satellite platforms, including Landsat, Sentinel, and MODIS, GEE offers numerous algorithms, such as support vector machines (SVM), random forest (RF), and decision trees, along with its own integrated code library [30-33].

Longoz forests are increasingly threatened by activities such as aquaculture, urbanization, agriculture, and the exploitation of forest resources. Aquaculture has been one of the primary drivers of longoz forest destruction during the latter half of the twentieth century [34]. The fertile soil surrounding longoz forests has made them vulnerable to unsustainable agricultural practices and deforestation, which significantly contribute to the reduction of forested areas. Longoz forests, with their rich ecosystems and biodiversity, are among the critical forest areas requiring conservation and sustainable management. Consequently, research conducted in these forests holds significant importance.

There are many studies using RS techniques to monitor forests. Vatandaslar et al. [35] conducted a study to model and map above-ground carbon (AGC) stocks in the İğneada Longoz Forest located in the Thrace region of Türkiye, using ALOS/PALSAR-2 SAR data. Horizontal polarization and the cross-polarization ratio (CPR) bands were identified as the most influential variables, with nonlinear modelling being preferred. The research revealed an average AGC density of 124 ± 115.4 t C ha^{-1} and identified a total carbon stock of 279,258.9 t. Reddy et al. [36] classified the vegetation and forest types of India using IRS Resourcesat-2 AWiFS data, identifying 29 land use/land cover classes, including 14 forest types and 7 shrubland types. They found that tropical dry deciduous (34.80%) and tropical moist deciduous forests (33.19%) were the dominant types, with India's natural vegetation covering 29.36% of its total geographical area. Their study resulted in comprehensive vegetation and forest type maps based on critical inputs. In addition to these, there are various studies focusing on mangrove forests, which are vital coastal ecosystems with significant ecological and carbon storage functions. Diniz et al. [2] analysed the annual changes in the status of Brazil's mangrove forests from 1985 to 2018 using the GEE platform. The study revealed that mangrove forest areas showed an increasing trend between 1985 and 1998. However, from 1999 to 2018, a 2% loss of mangrove forest area was observed. Li et al. [1] analysed the annual changes in the status of Brazil's mangrove forests from 1985 to 2018 using the GEE platform. The study revealed that mangrove forest areas showed an increasing trend between 1985 and 1998. However, from 1999 to 2018, a 2% loss of mangrove forest area was observed. Wan et al. [6] proposed a small-patched convolutional neural network (CNN) as an alternative to the traditional CNN to reduce the large input data in mapping mangrove species. The proposed method yielded more successful results compared to the traditional approach. Ghosh et al. [37] proposed a methodology to determine the canopy height of mangrove forests using RF and symbolic regression (SR) machine learning algorithms applied to synthetic aperture radar (SAR) and optical imagery. The study examined the potential of Sentinel-1 interferometric coherence and Sentinel-2 biophysical parameters for estimating canopy height in the Bhitarkanika Wildlife Sanctuary. The results indicated a reasonable correlation between interferometric coherence, biophysical variables, and canopy height, particularly with the Leaf Area Index (LAI) and Fraction of Vegetation Cover (FVC). Parida & Kumar [3] analysed the decadal changes in the mangrove forests along the Odisha coast of India using Landsat-5 and Sentinel-2A satellite data for the years 2009 and 2019, respectively. The satellite data were obtained and processed on the GEE platform. The study employed the SVM algorithm for classification purposes. The results revealed that the total mangrove area increased by 13.5%, from 222.43 km^2 in 2009 to 252.47 km^2 in 2019. Cipta et al. [5] determined the change areas in mangrove forests on the Belitung Islands between 1990 and 2020. For this purpose, Landsat 5, Landsat 7, and Landsat 8 images were used. The images were classified using the RF algorithm, along with the Modified Soil-Adjusted Vegetation Index (MSAVI), EVI, and NDVI plant indices on the GEE platform. The results indicated that the highest area in 2020 was 119.91 ha, with a classification accuracy of 99.09%. The lowest area, calculated as 70.88 ha in 2000, had a classification accuracy of 98.98%.

This study aims to assess the changes in the İğneada Longoz forests in Kırklareli Province, Türkiye, from 2000 to 2021, using Landsat-7 and Landsat-8 satellite imagery within the GEE platform. The analysis focuses on both the overall forest areas and the specific longoz forest areas, utilizing a custom-developed JavaScript code that employs RS techniques on GEE. The study further explores phenological changes in vegetation through NDVI and EVI time series analysis on the GEE platform. The developed methodology not only provides valuable insights into the temporal dynamics of the longoz forests but also serves as a critical tool for authorities, offering a framework for continuous monitoring and the identification of potential risks to the future of the İğneada Longoz forests. Unlike previous studies, which often provide limited temporal coverage or focus on broader forest typologies, this study uniquely combines long-term phenological analysis with spatially detailed forest classification specific to the İğneada Longoz ecosystem using cloud-based GEE tools.

2. Method

This study consists of two main sections. The first section focuses on the İğneada Longoz forests and the surrounding forests, treating them as a unified forest area, where a classification study was conducted, and the areas were calculated. This section includes nine steps: in the first step, satellite images from each year of the 21-year period (2000–2020) were selected; in the second and third steps, radiometric and sensor-related strip errors for Landsat 7 (ETM+) satellite images from 2004 to 2012 were corrected using the QGIS 3.16.0 software; in the fourth step, the boundaries of the current İğneada Longoz forests were derived from the 2020 İğneada stand map; in the fifth step, NDVI, EVI, and MNDWI values for each image were calculated; in the sixth step, a satellite image collection was created, followed by NDVI time series analysis; in the seventh step, each image was individually classified using the Random Forest Algorithm with supervised classification; in the eighth step, accuracy assessments were performed for each classified image; and in the ninth step, the classified images were transferred to ArcMAP 10.8 software, where vector transformation was applied, and the areas for each image were calculated. The second section aimed to distinguish the İğneada Longoz forests from the surrounding forests by performing classification using the current stand maps, and changes in the areas were determined.

2.1. Study area

This study was conducted in the İğneada Longoz forests, located within the Demirköy district of Kırklareli province, in the northwestern part of Türkiye. The İğneada Longoz forest is situated along the Black Sea coastline, near the Bulgarian border, and spans an area of 3,155 hectares. The area was designated as Türkiye's 39th National Park by a decision of the Council of Ministers, published in the Official Gazette on November 13, 2007. İğneada, the town where the National Park is located, is situated 27 km from Demirköy district, 97 km from the center of Kırklareli, and 237 km from Istanbul. The longoz forests are bordered by the Yıldız Mountains to the north. These forests provide significant biological diversity, supporting a rich ecosystem. The vegetation in the İğneada Longoz forests is composed of mixed tree species, including deciduous oak, hornbeam, alder, and beech. The National Park is home to 472 different plant species and serves as an important migration route for various bird species (http://igneada.tabiat.gov.tr/). The National Park is divided into two parts, with İğneada town located between them. The southern section of the park includes Saka Lake, Deniz Lake, Hamam Lake, Pedina Lake, Mert Lake, and the surrounding reed areas, along with longoz forests and deciduous forests. The northern part encompasses Erikli Lake and the surrounding reed areas, as well as longoz forests in the vicinity. The boundaries of the study area were determined using the 2020 stand map (Figure 1).

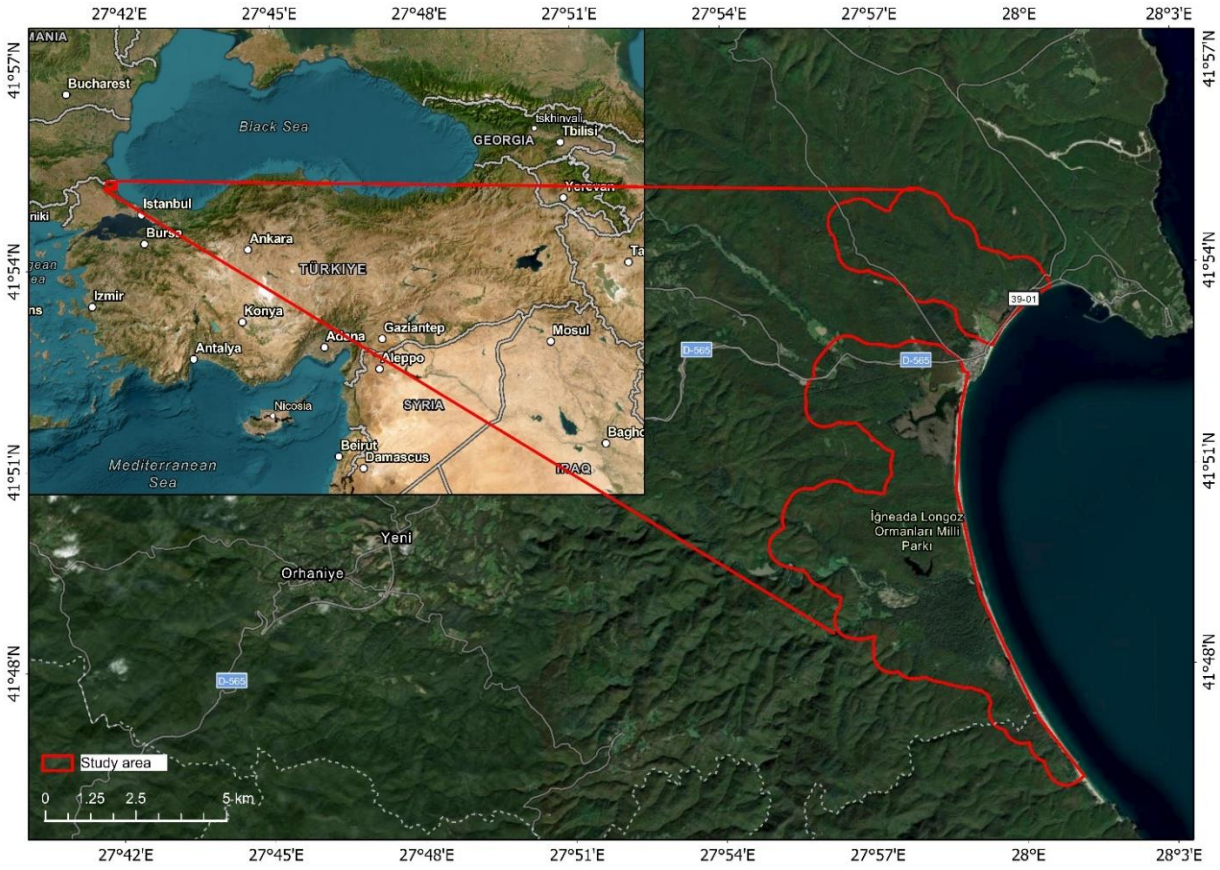


Figure 1. Study area map

2.2. Data sources

2.2.1. Satellite images

In this study, Landsat-7 (ETM+) and Landsat-8 (OLI) images were used. These systems were jointly developed through a collaboration between the United States Geological Survey (USGS) and the National Aeronautics and Space Administration (NASA). Landsat-7, equipped with the Advanced Thematic Mapper sensor, was launched into orbit on April 15, 1999. Satellite images have been missing data since June 2003 due to an error in the Scan Line Corrector (SLC). The Landsat 7 satellite is at an altitude of 705 km and has a temporal resolution of 16 days. It has 8 spectral bands, including panchromatic and thermal bands. Landsat 8, launched on February 11, 2013, operates at an altitude of approximately 705 km, similar to Landsat 7, and provides a 16-day temporal resolution. The satellite is equipped with an Operational Land Imager (OLI) and Thermal Infrared Sensor (TIRS), offering 9 spectral bands, including a panchromatic band. The primary reasons for utilizing Landsat satellite images in this study include their long-term data continuity, free and open access policy, adequate spatial and temporal resolution, and the availability of specific spectral bands suitable for land cover and vegetation analyses.

Due to incomplete data in Landsat 7 satellite images, the study utilized Landsat 7 imagery from 2000 to 2013 and Landsat 8 imagery from 2014 to 2020. This incompleteness stems from a malfunction in the Scan Line Corrector (SLC) of Landsat 7, which occurred in May 2003. The SLC failure resulted in systematic data gaps, particularly along the edges of the images, thereby reducing their suitability for comprehensive spatial analysis. GEE includes collections of radiometrically and geometrically corrected images. In years with no data deficiencies, Landsat 7 Collection 1 Tier 1 TOA Reflectance and Landsat 8 Collection 1 Tier 1 TOA Reflectance imagery were utilized. Radiometric correction of satellite images from 2004 to 2013, where data deficiencies occurred, was performed using QGIS software, and gap-affected portions of the imagery were addressed using reconstruction techniques prior to analysis. The corrected images were transferred to the GEE environment. Satellite images for each year were selected from cloudless images captured between March and September, corresponding to the season when the trees are green and the water levels in the longoz forests rise. The spectral and spatial resolution details of the images are provided in Table 1.

Table 1. Satellite images and their features

Landsat-7 (ETM+)			Landsat-8 (OLI)		
Band	Wavelength (μm)	Spatial resolution (m)	Band	Wavelength (μm)	Spatial resolution (m)
B1 (Blue)	0.45 – 0.52	30	B2(Blue)	0.45 – 0.51	30
B2 (Green)	0.52 – 0.60	30	B3 (Green)	0.53 – 0.59	30
B3 (Red)	0.63 – 0.69	30	B4(Red)	0.64 – 0.67	30
B4 (NIR)	0.77 – 0.90	30	B5(NIR)	0.85 – 0.88	30
B5 (SWIR)	1.55 – 1.75	30	B6(SWIR 1)	1.57 – 1.65	30

2.3. Indices used

In this study, NDVI and EVI indices were used for classification purposes and time series analysis. NDVI was developed by Rouse et al. [38] NDVI is the difference between the near infrared and visible reflectance values. NDVI values range from -1.0 to +1.0, with positive values indicating green vegetation and negative values representing non-vegetated surfaces, such as water, barren land, ice, snow, or clouds [39-41]. NDVI values were calculated using Equation (1). The EVI was designed to optimize the vegetation signal by improving sensitivity in high-biomass regions and enhancing vegetation monitoring through the separation of the canopy background signal and the reduction of atmospheric effects [16]. In this study, EVI values were calculated using Equation (2). The MNDWI index was incorporated into the classification to enhance the extraction of water bodies, particularly within longoz forests, from other landscape features. To improve the distinction between land and water in turbid and green waters, the near-infrared band was utilized to address reflection differences caused by shaded areas in urban environments, leading to the proposal of the MNDWI index [17]. Due to reflection differences caused by shaded areas in residential regions, as well as in turbid and green waters, the near-infrared band was replaced with the mid-infrared band to enhance the distinction between land and water, resulting in the proposal of the MNDWI. MNDWI was calculated with Equation (3).

$$NDVI = \frac{NIR - RED}{NIR + RED} \tag{1}$$

$$EVI = 2 \times \frac{NIR - RED}{NIR + 6 \times RED - 7.5 \times BLUE + 1} \tag{2}$$

$$MNDWI = \frac{GREEN - SWIR}{GREEN + SWIR} \tag{3}$$

2.4. Time series analysis

Time series analysis of remote sensing (RS) data reveals that land cover changes do not always occur in a progressive and gradual manner but can exhibit periods of rapid and abrupt transitions. These changes may be followed by either a swift recovery of ecosystems or an unstable trajectory [42]. NDVI time series analysis is well-suited for monitoring complex and long-term vegetation changes. In addition to capturing long-term

trends, interannual variations in vegetation dynamics can provide valuable insights into vegetation responses to meteorological events, such as drought. In this study, EVI time series analysis has also been incorporated alongside NDVI. The fundamental representation of the time series is presented in Equation (4).

$$p_t;\ t = \ t_0 \dots t_N \tag{4}$$

where, p_t represents a scalar pixel value at time t. t_0 is the smallest, and t_N is the largest time in the series.

2.5. Random forest algorithm

Random Forest is a widely used ensemble learning algorithm based on decision trees, often used in classification and regression tasks. It works by creating many individual decision trees during the training phase and aggregating their outputs to produce a more accurate and robust prediction [43]. Each tree in the forest is trained on a random subset of the original data, both in terms of samples (via bootstrap sampling) and features (via random feature selection at each node), which reduces the risk of overfitting and increases the generalizability of the model [44]. The final classification result is usually determined by a majority vote among all trees. Due to its high accuracy, ability to handle large high-dimensional datasets, and robustness to noise and outliers, Random Forest has become the method of choice in remote sensing applications such as land cover classification and vegetation mapping [10].

2.6. Classification process

The change in the İğneada Longoz forests was studied for the period from 2000 to 2020. NDVI and EVI time series analyses for the same years were also examined. The classification of all images used in the study was performed on the GEE platform. Scan line error in Landsat-7 satellite images were corrected using QGIS software. After performing radiometric correction on the images using the same software, they were imported into the GEE platform. Separate ImageCollections were created for each satellite platform used. After applying various filters, such as cloud and time, to the ImageCollections, the median statistic was calculated to obtain a single image for each year. Spring months were specifically preferred for classification to avoid cloud coverage. The study area was divided into nine classes based on land use: longoz, forest, agricultural land, lake, bare land, settlement, beach, sea, and reed bed. A pixel-based supervised classification approach was used in the study, employing the commonly used RF machine learning algorithm. The workflow of the classification process is shown in Figure 4. The accuracy of the classification was assessed using higher resolution Google Earth images for each year. Approximately 500 random points were placed on the images, and a binary comparison was made for each class between the classified image and the Google Earth image, resulting in the creation of a confusion matrix. Based on the confusion matrix, producer accuracy, user accuracy, overall accuracy, and kappa statistics were calculated. The process steps of the study are shown in Figure 2.

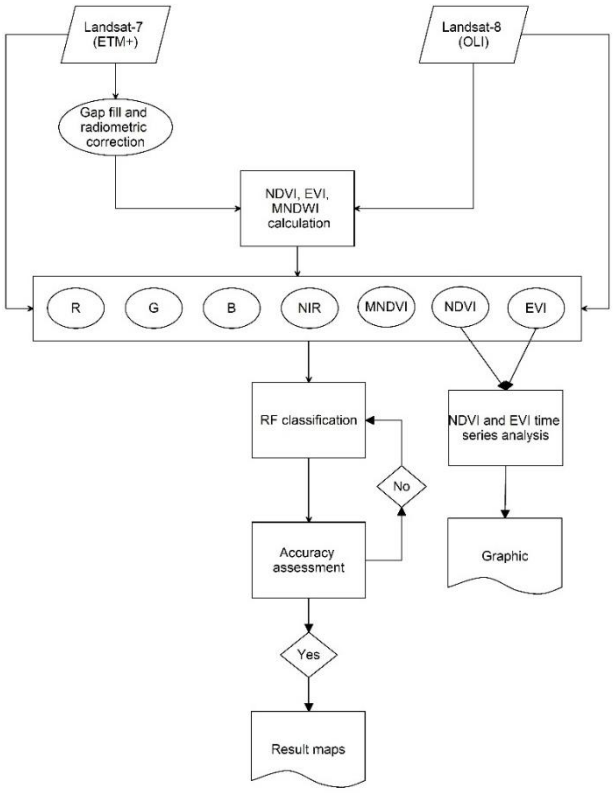


Figure 2. Workflow diagram

3. Results

3.1. Classification and time series analysis of the entire study area

In this study, which aimed to detect changes by distinguishing the İğneada Longoz forests and surrounding forested areas, pixel-based supervised classification was performed using the RF algorithm on Landsat-7 (ETM+) and Landsat-8 (OLI) satellite imagery. To enhance the delineation of forested areas, NDVI, EVI, and MNDWI indices were incorporated into the classification alongside the RGB and NIR bands. Accuracy analyses were conducted for a total of 26 images, including 21 from the first stage and 5 from the second stage. Classification maps are presented in Figure 3 at five-year intervals

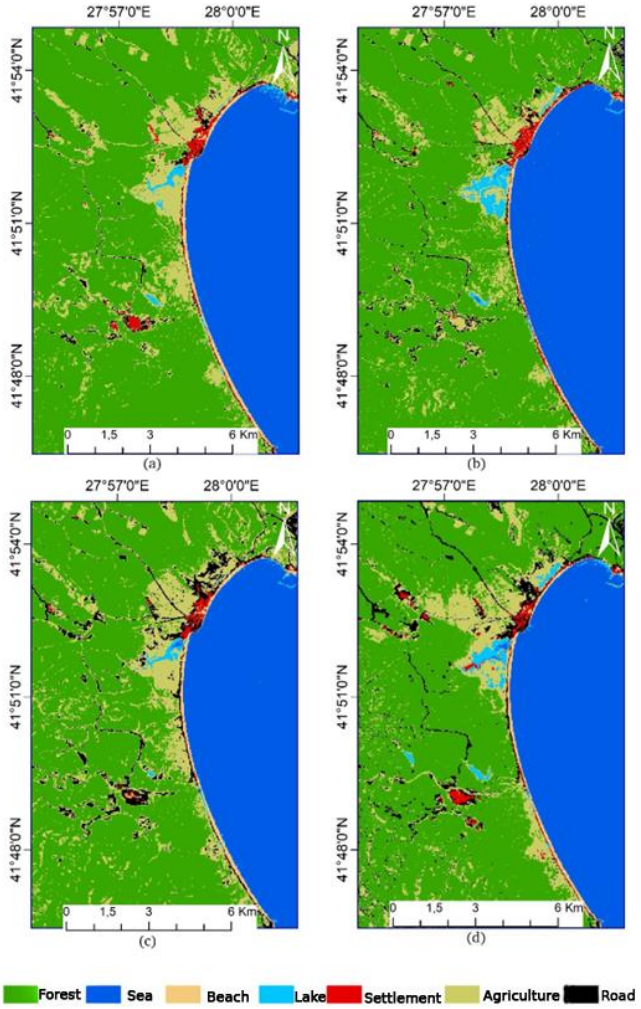


Figure 3. Classification maps

An examination of the spatial distribution of the classification maps reveals that forested areas dominate a significant portion of the study area. It was also observed that residential areas and agricultural lands are prominent, particularly along the coastal region. The changes in the areas of the classified categories are provided in Table 2.

Table 2. Area data of the entire forest area in the study area by year

Date	Forest area (ha)	Date	Forest area (ha)
2000	10,032.84	2011	9,926.55
2001	10,279.18	2012	9,619.65
2002	9,418.05	2013	9,482.22
2003	9,445.45	2014	9,949.50
2004	9,356.58	2015	9,912.78
2005	9,147.69	2016	9,522.00
2006	9,403.16	2017	10,103.04
2007	9,896.31	2018	9,376.02
2008	10,578.61	2019	10,251.81
2009	9,472.41	2020	6,229.89
2010	8,505.99		

The changes in forested areas are illustrated in Figure 4. No significant alterations in forested areas were observed between 2000 and 2019. The fluctuations noted in 2008 and 2010 were attributed to seasonal effects, leading to spectral similarities between classes and resulting in misclassifications

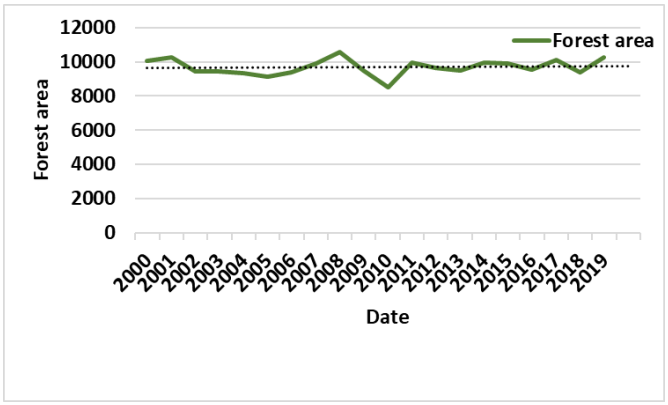


Figure 4. Change graph of forest areas

The classification accuracies for this study are presented in Table 3. It was observed that the overall accuracy (OA) exceeded 80% in nearly all years, with Kappa values consistently above 0.700. These results indicate that the classification can be considered highly successful

Table 3. Classification overall accuracy and kappa statistics values

Image date	OA (%)	Kappa
23.06.2000	88.17	0.846
10.06.2001	85.99	0.785
15.07.2002	87.99	0.831
15.05.2003	79.97	0.721
21.08.2004	84.72	0.798
05.06.2005	83.33	0.784
23.05.2006	85.68	0.808
30.08.2007	88.69	0.840
28.05.2008	90.63	0.877
31.05.2009	86.25	0.822
02.05.2010	84.99	0.782
09.08.2011	85.33	0.817
07.05.2012	83.12	0.780
06.08.2013	86.92	0.829
08.07.2014	85.91	0.814
27.07.2015	86.83	0.835
11.06.2016	87.72	0.851
30.06.2017	84.89	0.816
30.04.2018	85.12	0.817
19.05.2019	85.37	0.820

Vegetation index time series are potentially useful for examining vegetation dynamics, providing indicators of average vegetation levels and phenological cycles over the analysed period. In this study, NDVI and EVI time series analyses were conducted using the JavaScript language on the GEE platform (Figure 5). The analysis, covering the spring and summer seasons between 2000 and 2021, revealed an overall increasing trend. Notable fluctuations were observed, including sharp declines in 2008 and 2011, and increases in 2006, 2008, and 2009. The periods of sharp declines coincided with seasonally dry years. While no significant changes were detected in

forest areas classified as such, the NDVI and EVI time series indicated a general trend of increasing vegetation density in the study area over the years.

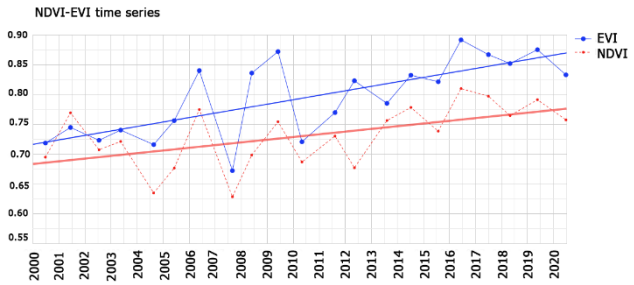


Figure 5. NDVI and EVI time series graph

Time series analysis and classification methods are frequently used with RS to detect forest areas. In this study, according to the NDVI-EVI time series graph for the forest class, the minimum value for NDVI is 0.629, and the maximum is 0.810, while for EVI, the minimum value is 0.672, and the maximum is 0.892. The years with minimum and maximum NDVI and EVI values are the same. The selection of the months in which the satellite images are chosen is crucial for the analysis. Based on the NDVI-EVI time series graph for the floodplain forests, the values obtained for NDVI range from a minimum of 0.645 to a maximum of 0.775, and for EVI, from a minimum of 0.729 to a maximum of 0.850. Both NDVI and EVI provided equivalent results in this case.

Additionally, the correlation between pixel values calculated using both indices was determined, with an R value of 0.788 and an R^2 value of 0.621 (Figure 6). These results indicate a strong correlation between the two indices. Given this strong correlation, it can be confidently stated that both NDVI and EVI indices can be interchangeably utilized for vegetation phenological studies.

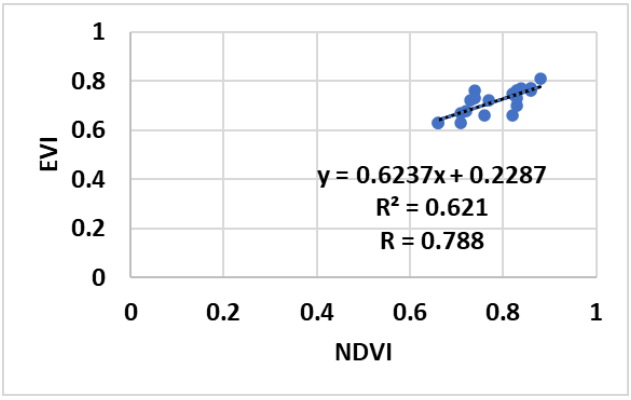


Figure 6. Correlation graph of NDVI and EVI indices

3.2. Classification İğneada Longoz forest areas

At this stage, the changes in the longoz forests were examined approximately every five years, considering the cloud cover conditions of satellite images, for the years 2000, 2004, 2010, 2015, and 2021. To distinguish between the longoz forests and surrounding forests, classification was performed using the forest inventory map obtained from the Ministry of Agriculture and Forestry of the Republic of Türkiye. Since the forest inventory map shows the updated boundaries of the İğneada Longoz forests, the most accurate result was obtained from the satellite image of 2021. Unlike the classification in the first section, the road class was excluded, and the reed and bare land classes were added to the analysis. These changes were made to better represent the study area. The classification maps are provided in Figure 7. The longoz forest area changes derived from the classification map are shown in Table 4.

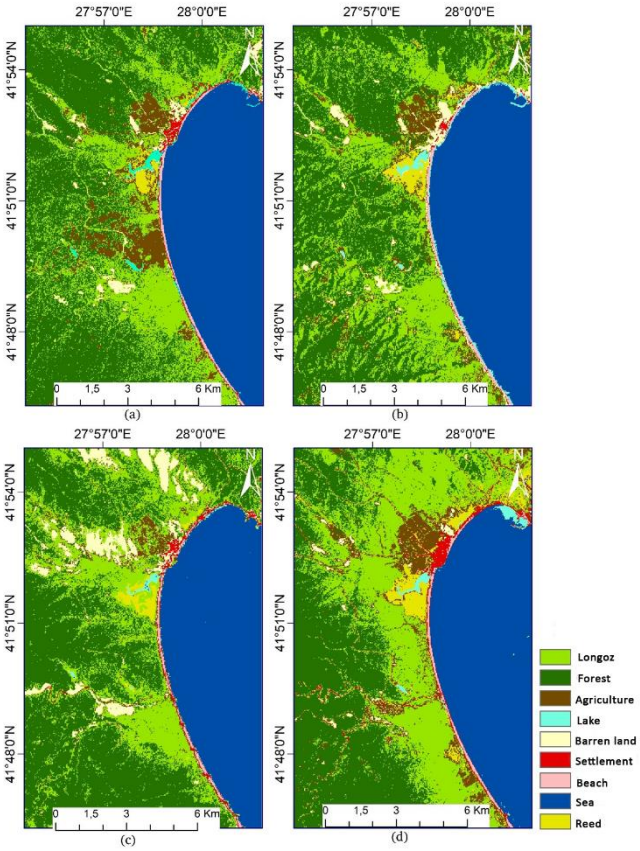


Figure 7. Longoz forests classification map

Table 4. Longoz forest area

Date	Igneada Longoz areas (ha)
2000	3575.79
2004	4003.02
2010	3629.61
2015	4790.61
2021	3290.94

When examining the changes in longoz forest areas between 2000 and 2021, a radical change is noticeable in 2015. However, considering the size of the area, it is thought that forest areas may have been misclassified as longoz forests. Nevertheless, especially in 2021, some growth in the urban areas along the coastal zone in the northern part of the study area contributed to the reduction of the longoz forest areas.

The classified satellite images were processed in ArcMAP 10.8 software, where raster-to-vector conversion was applied to calculate forest areas. As a result of the calculation, the total forest area ranged from 10,251.81 hectares to 6,229.89 hectares, while the

change in floodplain forest areas was observed between 3,290.94 hectares and 4,790.61 hectares. In the first stage of classification, the most confused pairs based on the error matrices were coastal areas-settlement areas and road-agriculture areas. The resolution of the satellite images was occasionally insufficient for the extraction of coastal areas and roads.

The calculation of the accuracy of the classification study of longoz forests at an average of five-year intervals is given in Table 5.

Table 5. Classification accuracy assessment of longoz forests

Image date	OA (%)	Kappa
23.06.2000	81.46	0.750
21.08.2004	75.92	0.649
02.05.2010	84.14	0.783
27.07.2015	89.88	0.863
27.07.2021	90.04	0.866

When examining Table 5, the OA value was lowest in 2004 at 75.92%, while it was highest in 2021 at 90.04%. Although the classification accuracies indicate the OA, spectral mixing is unavoidable, especially in distinguishing forest areas from longoz areas.

4. Discussion

In Türkiye, Bozkaya [45] conducted a temporal assessment and future modelling study of the İğneada Longoz forests. Toker [46] carried out a change detection study for İğneada from 1987 to 2017. The results obtained both studies are consistent with the values presented in this thesis. In all three studies, it has been observed that the İğneada Longoz forests have decreased. The results of these two studies are compatible with the results of our study. All three studies revealed that İğneada Longoz forests are decreasing.

Gencal et al. [47] conducted a study on the change detection of the Karacabey Longoz Forests in Bursa, Türkiye, for the years 2010 and 2017. Arekhi et al. [48] performed a time series analysis for İğneada using Landsat-8 and Sentinel-2A data. Cipta et al. [5] studied the changes in longoz forests in the Bangka Belitung Archipelago between 1990 and 2020 using Landsat-5, Landsat-7, and Landsat-8 satellite imagery. They performed the study using MSAVI, NDVI, and EVI indices on the GEE platform. This study is quite like our research. The study concluded that the longoz forests decreased from 1990 to 2000 and then increased again up to 2020. The accuracy of the study was determined using a confusion matrix, like our approach. The OA of the classifications was nearly 100%. In a study by Parida & Kumar [3] the changes in longoz forests in India between 2009 and 2019 were analysed using Landsat-5 and Sentinel-2 imagery on the GEE platform. The classification, performed using the SVM algorithm, revealed a 13.5% increase in forested areas. In this study, as in ours, the OA values exceeded 85%. Similar to the other studies, this research also demonstrated the effectiveness of using Landsat imagery and the GEE platform for monitoring longoz forests. Although some of these studies reported higher accuracy values the differences can be attributed to factors such as smaller study areas, less spectral heterogeneity, or different classification algorithms (e.g., SVM vs. RF). Our study covered a larger and ecologically complex area, which may lead to slightly lower but still acceptable classification performance.

In our study, two vegetation and water-related indices—NDVI, EVI, and MNDWI—played a crucial role in accurately detecting changes in the longoz forest ecosystem. NDVI was used to highlight vegetation density and health by capturing the contrast between red and near-infrared reflectance, making it particularly effective in assessing overall vegetation dynamics. EVI, on the other hand, was employed to reduce atmospheric and canopy background noise, providing improved sensitivity in high biomass regions such as longoz forests. Meanwhile, MNDWI allowed us to better delineate water bodies within and around the forest, which is vital for distinguishing flooded forest areas from dense vegetation. These indices complemented each other by offering a more nuanced understanding of the complex interactions between vegetation and hydrological conditions in longoz ecosystems, thereby enhancing classification accuracy and environmental interpretation.

This study also has certain limitations. Seasonal image availability and cloud coverage affected the consistency of temporal analysis. Additionally, due to the limited number of in-situ ground truth data, the validation process relied primarily on visual interpretation and high-resolution imagery, which might slightly reduce the accuracy of the reference data. Another significant limitation is the SLC in the Landsat-7 imagery after 2003, which caused data gaps and required preprocessing steps to mitigate missing data. Despite these efforts, some spatial inconsistencies may have influenced the classification results for certain years.

5. Conclusion

This study has demonstrated that the GEE platform is highly useful for tracking longoz forests. Additionally, the GEE cloud computing platform provides significant advantages, especially in processing large datasets and storing geographic data. It allows analysis of these data on any platform with internet access, independent of hardware. In this study conducted on GEE, it was observed that there has been no dramatic change in the longoz forest area of İğneada over the last 21 years. According to the classification results, the forest area in 2019 decreased by 2.18% compared to the year 2000. When examining the 21-year NDVI and EVI time series graph, a continuous upward trend in vegetation cover was identified. The time series obtained from both indices are nearly parallel to each other. It was concluded that these two indices can be used interchangeably and are highly beneficial for monitoring plant phenological structures. Although no phenological species distinction was made in this study through time series analysis, it proves highly valuable for tracking changes in vegetation density. Thanks to the developed JavaScript code, this

study will enable easy tracking of İğneada Longoz forests and their plant phenological cycle over time.

Acknowledgement

This study was produced from the master's thesis of the first author.

Author contributions

First author, third author, and **second author** designed the study. **First author** reviewed the literature and collected data**. First author** and **second author** performed the analysis. **third author** and **second author** assisted in writing.

Conflicts of interest

The authors declare no conflicts of interest.

References

1. Li, H., Jia, M., Zhang, R., Ren, Y., & Wen, X. (2019). Incorporating the plant phenological trajectory into mangrove species mapping with dense time series Sentinel-2 imagery and the Google Earth Engine platform. Remote Sensing, 11(21). https://doi.org/10.3390/rs11212479
2. Diniz, C., Cortinhas, L., Nerino, G., Rodrigues, J., Sadeck, L., Adami, M., & Souza-Filho, P. W. M. (2019). Brazilian mangrove status: Three decades of satellite data analysis. Remote Sensing, 11(7), 808. https://doi.org/10.3390/rs11070808
3. Parida, B. R., & Kumar, P. (2020). Mapping and dynamic analysis of mangrove forest during 2009–2019 using landsat–5 and sentinel–2 satellite data along Odisha Coast. Tropical Ecology, 61(4), 538–549. https://doi.org/10.1007/s42965-020-00112-7
4. Twilley, R. R., Rovai, A. S., & Riul, P. (2018). Coastal morphology explains global blue carbon distributions. Frontiers in Ecology and the Environment, 16(9), 503–508.
5. Cipta, I. M., Sobarman, F. A., Sanjaya, H., & Darminto, M. R. (2021). Analysis of Mangrove Forest Change from Multioral Landsat Imagery Using Google Earth Engine Application: (Case Study: Belitung Archipelago 1990 - 2020). 2021 IEEE Asia-Pacific Conference on Geoscience, Electronics and Remote Sensing Technology, AGERS 2021-Proceeding, 90–95. https://doi.org/10.1109/AGERS53903.2021.9617354
6. Wan, L., Zhang, H., Lin, G., & Lin, H. (2019). A small-patched convolutional neural network for mangrove mapping at species level using high-resolution remote-sensing image. Annals of GIS, 25(1), 45–55. https://doi.org/10.1080/19475683.2018.1564791
7. Topaloglu, R. H. (2022). Investigation of Land Use/Land Cover change in Mersin using geographical object-based image analysis (GEOBIA). Advanced Remote Sensing, 2(2), 40–46. https://publish.mersin.edu.tr/index.php/arsej/article/view/247
8. Gull, A., & Mahmood, S. (2022). Spatio-temporal analysis and trend prediction of land cover changes using markov chain model in Islamabad, Pakistan. Advanced GIS, 2(2), 52–61. https://publish.mersin.edu.tr/index.php/agis/article/view/679
9. Nsiah, R. A., Mantey, S., & Ziggah, Y. Y. (2024). Assessing the contribution of RGB VIs in improving building extraction from RGB-UAV images. Mersin Photogrammetry Journal, 6(1), 9–21. https://doi.org/10.53093/mephoj.1399083
10. Jin, Y., Liu, X., Chen, Y., & Liang, X. (2018). Land-cover mapping using Random Forest classification and incorporating NDVI time-series and texture: A case study of central Shandong. International Journal of Remote Sensing, 39(23), 8703–8723. https://doi.org/10.1080/01431161.2018.1490976
11. Cheret, V., & Denux, J.-P. (2011). Analysis of MODIS NDVI time series to calculate indicators of Mediterranean forest fire susceptibility. GIScience & Remote Sensing, 48(2), 171–194.
12. Chao Rodríguez, Y., El Anjoumi, A., Domínguez Gómez, J. A., Rodríguez Pérez, D., & Rico, E. (2014). Using Landsat image time series to study a small water body in Northern Spain. Environmental Monitoring and Assessment, 186(6), 3511–3522. https://doi.org/10.1007/s10661-014-3634-8
13. Chen, B., Xiao, X., Li, X., Pan, L., Doughty, R., Ma, J., Dong, J., Qin, Y., Zhao, B., Wu, Z., Sun, R., Lan, G., Xie, G., Clinton, N., & Giri, C. (2017). A mangrove forest map of China in 2015: Analysis of time series Landsat 7/8 and Sentinel-1A imagery in Google Earth Engine cloud computing platform. ISPRS Journal of Photogrammetry and Remote Sensing, 131, 104–120. https://doi.org/10.1016/j.isprsjprs.2017.07.011
14. Johansen, K., Phinn, S., & Taylor, M. (2015). Mapping woody vegetation clearing in Queensland, Australia from Landsat imagery using the Google Earth Engine. Remote Sensing Applications: Society and Environment, 1, 36–49. https://doi.org/10.1016/j.rsase.2015.06.002
15. Unel, F. B., Kusak, L., & Yakar, M. (2023). GeoValueIndex map of public property assets generating via Analytic Hierarchy Process and Geographic Information System for Mass Appraisal: GeoValueIndex. *Aestimum*, *82*, 51-69.
16. Huete, A., Didan, K., Miura, T., Rodriguez, E. P., Gao, X., & Ferreira, L. G. (2002). Overview of the radiometric and biophysical performance of the MODIS vegetation indices. Remote Sensing of

Environment, 83(1–2). https://doi.org/10.1016/S0034-4257(02)00096-2
17. Xu, H. (2006). Modification of normalised difference water index (NDWI) to enhance open water features in remotely sensed imagery. International Journal of Remote Sensing, 27(14), 3025–3033. https://doi.org/10.1080/01431160600589179
18. Hawick, K. A., Coddington, P. D., & James, H. A. (2003). Distributed frameworks and parallel algorithms for processing large-scale geographic data. Parallel Computing, 29(10), 1297–1333.
19. Başara, A. C., Tabar, M. E., Gülsün, S., & Şişman, Y. (2022). Monitoring Urban Sprawl in Atakum District Using CORINE Data. Advanced Geomatics, 2(2), 49–56. https://publish.mersin.edu.tr/index.php/geomatics/article/view/481
20. Ünel, F. B., Kuşak, L., Yakar, M., & Doğan, H. (2023). Coğrafi bilgi sistemleri ve analitik hiyerarşi prosesi kullanarak Mersin ilinde otomatik meteoroloji gözlem istasyonu yer seçimi. *Geomatik*, *8*(2), 107-123.
21. Binuyo, O., & Bello, V. A. (2024). Spatial association in students' residential apartment property characteristics around a university. Advanced GIS, 4(2), 82–99. https://publish.mersin.edu.tr/index.php/agis/article/view/1558
22. Türk, T., & Demirel, Y. (2024). Automatic detection of active fires and burnt areas in forest areas using optical satellite imagery and deep learning methods. Mersin Photogrammetry Journal, 6(2), 66–78. https://doi.org/10.53093/mephoj.1575877
23. Mahdavifard, M., Ahangar, S. K., Feizizadeh, B., Kamran, K. V., & Karimzadeh, S. (2023). Spatio-Temporal monitoring of Qeshm mangrove forests through machine learning classification of SAR and optical images on Google Earth Engine. International Journal of Engineering and Geosciences, 8(3), 239–250. https://doi.org/10.26833/IJEG.1118542
24. Yılmaz, O. S., Gülgen, F., Güngör, R., & Kadi, F. (2018). Coğrafi Bilgi Sistemleri ve Uzaktan Algılama Teknikleri İle Arazi Kullanım Değişiminin İncelenmesi, Köprübaşı İlçesi Örneği. Geomatik. https://doi.org/10.29128/geomatik.410987
25. Güngör, R., Uzar, M., Atak, B., Yılmaz, O. S., & Gümüş, E. (2022). Orthophoto production and accuracy analysis with UAV photogrammetry. Mersin Photogrammetry Journal, 4(1), 1–6. https://doi.org/10.53093/mephoj.1122615
26. Yakar, M., Yıldız, F., Uray, F., & Metin, A. (2010, June). Photogrammetric Measurement of The Meke Lake and Its Environment with Kite Photographs to Monitoring of Water Level to Climate Change. In *ISPRS Commission V Mid-Term Symposium* (pp. 613-616).
27. Yılmaz, O. S. (2023). Frekans oranı yöntemiyle coğrafi bilgi sistemi ortamında heyelan duyarlılık haritasının üretilmesi: Manisa, Demirci, Tekeler Köyü örneği. Geomatic, 8(1), 42–54. https://doi.org/10.29128/geomatik.1108735
28. Kadı, F., & Yılmaz, O. S. (2024a). Determination of alternative forest road routes using produced landslide susceptibility maps: A case study of Tonya (Trabzon), Türkiye. International Journal of Engineering and Geosciences, 9(2), 147–164. https://doi.org/10.26833/ijeg.1355615
29. Kadı, F., & Yılmaz, O. S. (2024b). Orman içi açıklıklara ait zamansal değişimlerin uzaktan algılama teknikleri ile Google Earth Engine platformunda tespit edilmesi: Trabzon-Düzköy İlçesi örneği. Geomatik, 9(2), 141–155. https://doi.org/10.29128/geomatik.1363873
30. Avci, C., Budak, M., Yagmur, N., & Balcik, F. B. (2023). Comparison between random forest and support vector machine algorithms for LULC classification. International Journal of Engineering and Geosciences, 8(1), 1–10. https://doi.org/10.26833/IJEG.987605
31. Yılmaz, O. S., Gülgen, F., & Ateş, A. M. (2023). Determination of the appropriate zone on dam surface for floating photovoltaic system installation using RS and GISc technologies. International Journal of Engineering and Geosciences, 8(1), 63–75. https://doi.org/10.26833/IJEG.1052556
32. Yılmaz, O. S., Özkan, G., & Gülgen, F. (2021). Determining highway slope ratio using a method based on slope angle calculation. International Journal of Engineering and Geosciences, 6(2), 98–103. https://doi.org/10.26833/IJEG.704317
33. Amani, M., Ghorbanian, A., Ahmadi, S. A., Kakooei, M., Moghimi, A., Mirmazloumi, S. M., Moghaddam, S. H. A., Mahdavi, S., Ghahremanloo, M., Parsian, S., Wu, Q., & Brisco, B. (2020). Google Earth Engine Cloud Computing Platform for Remote Sensing Big Data Applications: A Comprehensive Review. IEEE Journal of Selected Topics in Applied Earth Observations and Remote Sensing, 13, 5326–5350. https://doi.org/10.1109/JSTARS.2020.3021052
34. Friess, D. A., Rogers, K., Lovelock, C. E., Krauss, K. W., Hamilton, S. E., Lee, S. Y., Lucas, R., Primavera, J., Rajkaran, A., & Shi, S. (2019). The State of the World's Mangrove Forests: Past, Present, and Future. Annual Review of Environment and Resources, 44(April 2021), 89–115. https://doi.org/10.1146/annurev-environ-101718-033302
35. Vatandaslar, C., Bolat, F., Abdikan, S., Pamukcu-Albers, P., & Satiral, C. (2020). i Forest. IForest - Biogeosciences and Forestry, 17, 277–285. https://doi.org/10.3832/ifor4527-017
36. Reddy, C. S., Jha, C. S., Diwakar, P. G., & Dadhwal, V. K. (2015). Nationwide classification of forest

types of India using remote sensing and GIS. Environmental Monitoring and Assessment, 187(12), 1–30. https://doi.org/10.1007/s10661-015-4990-8
37. Ghosh, S. M., Behera, M. D., & Paramanik, S. (2020). Canopy height estimation using sentinel series images through machine learning models in a Mangrove Forest. Remote Sensing, 12(9), 1519. https://doi.org/10.3390/RS12091519
38. Rouse, J. W., Haas, R. H., Schell, J. A., & Deering, D. W. (1974). Monitoring Vegetation Systems in the Great Plains with Erts. NASA Spec, 351, 309.
39. Eidenshink, J. C. (1992). The 1990 conterminous US AVHRR data set. Photogrammetric Engineering & Remote Sensing, 58(6), 809–813.
40. Yilmaz, H. M., Yakar, M., Mutluoglu, O., Kavurmaci, M. M., & Yurt, K. (2012). Monitoring of soil erosion in Cappadocia region (Selime-Aksaray-Turkey). *Environmental Earth Sciences*, *66*(1), 75-81.
41. Yakar, M., Yilmaz, H. M., & Yurt, K. (2010). The effect of grid resolution in defining terrain surface. *Experimental Techniques*, *34*(6), 23-29.
42. Lambin, E. F., Geist, H. J., & Lepers, E. (2003). Dynamics of land-use and land-cover change in tropical regions. Annual Review of Environment and Resources, 28, 205–241. https://doi.org/10.1146/annurev.energy.28.050302.105459
43. Breiman, L. (2001). Random Forests (Vol. 45).
44. Gislason, P. O., Benediktsson, J. A., & Sveinsson, J. R. (2006). Random Forests for land cover classification. Pattern Recognition Letters, 27(4), 294–300. https://doi.org/10.1016/J.PATREC.2005.08.011
45. Bozkaya, A. G. (2013). İğneada Koruma Alanının Uzaktan Algılama ve Coğrafi Bilgi Sistemleri ile Zamansal Değerlendirilmesi ve Geleceğe Yönelik Modellenmesi. İstanbul Teknik Üniversitesi.
46. Toker, M. (2018). Landsat ve Sentinel Uydu Görüntüleri Kullanılarak Zamansal Değişim Tespiti Analizi: Bir Vaka Çalışması- İğneada Taşkın Ormanı Milli Parkı. İstanbul Teknik Üniversitesi.
47. Gencal, B., Taş, İ., & Akay, A. E. (2018). Spatiotemporal Change Detection of the Linden Forests in Bursa, Turkey. European Journal of Forest Engineering, 4(2), 50–55. https://doi.org/10.33904/ejfe.495088
48. Arekhi, M., Goksel, C., Balik Sanli, F., & Senel, G. (2019). Comparative Evaluation of the Spectral and Spatial Consistency of Sentinel-2 and Landsat-8 OLI Data for Igneada Longos Forest. ISPRS International Journal of Geo-Information, 8(2), 56. https://doi.org/10.3390/ijgi8020056

© Author(s) 2026. This work is distributed under https://creativecommons.org/licenses/by-sa/4.0/